Supplemental Material: Theorem on the Compatibility of Spherical Kirigami Tessellations

Xiangxin Dang,[1] Fan Feng,[2] Huiling Duan,[1,3] and Jianxiang Wang[1,3,*]

[1] *State Key Laboratory for Turbulence and Complex Systems, Department of Mechanics and Engineering Science, College of Engineering, Peking University, Beijing 100871, China*
[2] *Cavendish Laboratory, University of Cambridge, Cambridge CB3 0HE, UK*
[3] *CAPT-HEDPS, and IFSA Collaborative Innovation Center of MoE, College of Engineering, Peking University, Beijing 100871, China*

(Dated: January 12, 2022)

I. KIRIGAMI STRIPS

We refer to SQK with more than two columns and rows as SQK tessellations, and those with only two columns or rows as SQK strips. A 10×2 SQK strip is illustrated in Fig. S1(a). The values of opening angles can be transmitted throughout the kirigami strip by the fact that each single quadrilateral void has one free opening angle and the opposite angles at the same vertex sum to π. For example, as shown in Fig. S1(b), we can see that $\gamma_1 + \beta_2 = \pi$ and $\delta_2 + \alpha_3 = \pi$. As a result, the kirigami strip can be continuously deployed with a single degree of freedom. The deformation formulation of the SQK strips can be included in the framework of general $M \times N$ SQK tessellations, which we will show below.

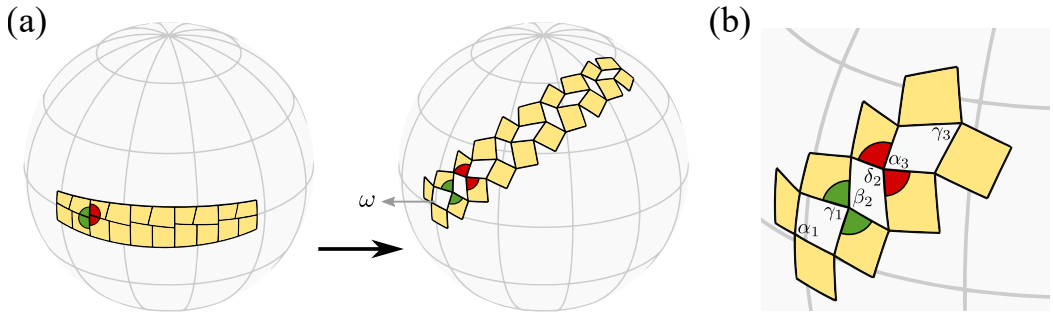

FIG. S1. SQK strips. (a) A SQK strip and its deployed configuration at $\omega = 0.5\pi$. (b) The opening angles can be transmitted over the slits by the constraints that the opposite angles of adjacent slits sum to π.

II. GEOMETRY OF A SINGLE SLIT

A single slit of SQK strips or tessellations is deployed to a convex spherical quadrilateral void. We use K to denote the Gaussian curvature of the sphere. As shown in Fig. S2, the spherical quadrilateral $F_2X_1F_1X_2$ is formed by the great-circle arcs $a, b, c, d \in (0, \pi/\sqrt{K})$ with opening angles $\alpha, \beta, \gamma, \delta \in (0, \pi)$. The quadrilateral void can be divided into two spherical triangles $F_2X_1X_2$ and $X_1F_1X_2$ by connecting the vertices X_1 and X_2 via a geodesic curve, or into spherical triangles $F_2X_1F_1$ and $F_2F_1X_2$ by connecting the vertices F_1 and F_2. Following the spherical cosine rules, we have

$$\cos(a\sqrt{K})\cos(d\sqrt{K}) + \sin(a\sqrt{K})\sin(d\sqrt{K})\cos\alpha = \cos(b\sqrt{K})\cos(c\sqrt{K}) + \sin(b\sqrt{K})\sin(c\sqrt{K})\cos\gamma, \tag{S1}$$

$$\cos(a\sqrt{K})\cos(b\sqrt{K}) + \sin(a\sqrt{K})\sin(b\sqrt{K})\cos\beta = \cos(c\sqrt{K})\cos(d\sqrt{K}) + \sin(c\sqrt{K})\sin(d\sqrt{K})\cos\delta. \tag{S2}$$

* jxwang@pku.edu.cn

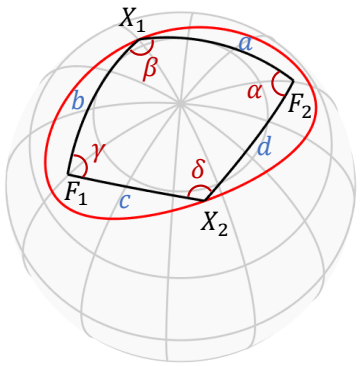

FIG. S2. Notations of a convex spherical quadrilateral void $F_2X_1F_1X_2$ of side lengths $a,\ b,\ c,\ d$, and opening angles $\alpha,\ \beta,\ \gamma,\ \delta$. This void is formed by a deployed slit of SQK strips or tessellations, so that the side lengths satisfy $a+b=c+d$. In addition, the quadrilateral void can be determined by two points $X_1,\ X_2$ on a spherical ellipse with foci $F_1,\ F_2$.

The differential forms of Eqs. (S1) and (S2) are

$$\frac{\mathrm{d}\gamma}{\mathrm{d}\alpha}=\frac{\sin\left(a\sqrt{K}\right)\sin\left(d\sqrt{K}\right)\sin\alpha}{\sin\left(b\sqrt{K}\right)\sin\left(c\sqrt{K}\right)\sin\gamma}, \tag{S3}$$

$$\frac{\mathrm{d}\delta}{\mathrm{d}\beta}=\frac{\sin\left(a\sqrt{K}\right)\sin\left(b\sqrt{K}\right)\sin\beta}{\sin\left(c\sqrt{K}\right)\sin\left(d\sqrt{K}\right)\sin\delta}. \tag{S4}$$

Denote the area of the spherical triangle $F_2X_1X_2$ as S_α. The area S_α can be determined by the side lengths a, d, and the included angle α:

$$\tan(KS_\alpha/2)=\frac{\tan(a\sqrt{K}/2)\tan(d\sqrt{K}/2)\sin\alpha}{1+\tan(a\sqrt{K}/2)\tan(d\sqrt{K}/2)\cos\alpha}. \tag{S5}$$

We will find the following trigonometric identities useful:

$$\sin(KS_\alpha)=\frac{2\tan(KS_\alpha/2)}{1+\tan^2(KS_\alpha/2)}, \tag{S6}$$

$$\cos(KS_\alpha)=\frac{1-\tan^2(KS_\alpha/2)}{1+\tan^2(KS_\alpha/2)}, \tag{S7}$$

$$\tan(KS_\alpha)=\frac{2\tan(KS_\alpha/2)}{1-\tan^2(KS_\alpha/2)}. \tag{S8}$$

We also have the following differential relationship:

$$\frac{\mathrm{d}(KS_\alpha)}{\mathrm{d}\alpha}=\cos^2\left(KS_\alpha\right)\frac{\mathrm{d}\tan(KS_\alpha)}{\mathrm{d}\alpha}. \tag{S9}$$

Substituting Eqs. (S5), (S7), (S8) into Eq.(S9) we obtain

$$A(\alpha,K)\triangleq 1-\frac{\mathrm{d}(KS_\alpha)}{\mathrm{d}\alpha}=\frac{\cos(a\sqrt{K})+\cos(d\sqrt{K})}{\sin(a\sqrt{K})\sin(d\sqrt{K})\cos\alpha+\cos(a\sqrt{K})\cos(d\sqrt{K})+1}. \tag{S10}$$

In the same way, we denote S_γ as the area of the spherical triangle $X_1F_1X_2$, and define the function $B(\gamma,K)$ by

$$B(\gamma,K)\triangleq 1-\frac{\mathrm{d}(KS_\gamma)}{\mathrm{d}\gamma}=\frac{\cos(b\sqrt{K})+\cos(c\sqrt{K})}{\sin(b\sqrt{K})\sin(c\sqrt{K})\cos\gamma+\cos(b\sqrt{K})\cos(c\sqrt{K})+1}. \tag{S11}$$

The interior angle summation and the spherical quadrilateral area have the following relationship:

$$\alpha+\beta+\gamma+\delta=2\pi+KS_\alpha+KS_\gamma. \tag{S12}$$

The differential form of Eq. (S12) is

$$\mathrm{d}\alpha + \mathrm{d}\beta + \mathrm{d}\gamma + \mathrm{d}\delta = \mathrm{d}(KS_\alpha) + \mathrm{d}(KS_\gamma). \tag{S13}$$

Eqs. (S1), (S2), (S12) indicate that the spherical quadrilateral void has a single degree-of-freedom upon deployment (three equations with four unknowns α, β, γ, δ). Substituting Eqs. (S3), (S4), (S10), (S11) into Eq. (S13), we obtain

$$\frac{\mathrm{d}\beta}{\mathrm{d}\alpha} + \frac{\sin(a\sqrt{K})\sin(b\sqrt{K})\sin\beta}{\sin(c\sqrt{K})\sin(d\sqrt{K})\sin\delta}\frac{\mathrm{d}\beta}{\mathrm{d}\alpha} + A(\alpha,K) + B(\gamma,K)\frac{\sin(a\sqrt{K})\sin(d\sqrt{K})\sin\alpha}{\sin(b\sqrt{K})\sin(c\sqrt{K})\sin\gamma} = 0. \tag{S14}$$

Besides, we have the identity

$$\frac{\sin(c\sqrt{K})\sin(d\sqrt{K})\sin\delta + \sin(a\sqrt{K})\sin(b\sqrt{K})\sin\beta}{B(\gamma,K)\sin(a\sqrt{K})\sin(d\sqrt{K})\sin\alpha + A(\alpha,K)\sin(b\sqrt{K})\sin(c\sqrt{K})\sin\gamma} = 1. \tag{S15}$$

We will prove Eq. (S15) later in Section III. Substituting Eq. (S15) into Eq. (S14), we obtain

$$\frac{\mathrm{d}\beta}{\mathrm{d}\alpha} = -\frac{\sin(d\sqrt{K})\sin\delta}{\sin(b\sqrt{K})\sin\gamma}. \tag{S16}$$

We define the relationship between α and β by

$$\cos\beta = \bar{g}(\cos\alpha; a, b, c, d, K). \tag{S17}$$

Since $\beta = \sphericalangle F_1X_1X_2 + \sphericalangle X_2X_1F_2$, we can use the spherical cosine rules and derive the explicit expression of $\bar{g}$:

$$\begin{aligned}
\bar{g}[\cos\alpha; a, b, c, d, K] = \cos\left\{\begin{array}{l} \arccos\left[\dfrac{\cos(c\sqrt{K}) - \cos(b\sqrt{K})\cos(e\sqrt{K})}{\sin(b\sqrt{K})\sin(e\sqrt{K})}\right] \\ +\arccos\left[\dfrac{\cos(d\sqrt{K}) - \cos(a\sqrt{K})\cos(e\sqrt{K})}{\sin(a\sqrt{K})\sin(e\sqrt{K})}\right]\end{array}\right\}, \\
e\sqrt{K} = \arccos[\cos(a\sqrt{K})\cos(d\sqrt{K}) + \sin(a\sqrt{K})\sin(d\sqrt{K})\cos\alpha],
\end{aligned} \tag{S18}$$

where e is the length of the diagonal X_1X_2. If the side lengths a, b, c, d are given, the opening angles β, γ, δ are uniquely and explicitly determined by α according to Eqs. (S1), (S2), (S17), and (S18). The derivative of $\bar{g}$ with respect to $\cos\alpha$ can be obtained from Eqs. (S16) and (S17):

$$\bar{g}'[\cos\alpha; a, b, c, d, K] = \frac{d\cos\beta}{d\cos\alpha} = -\frac{\sin(d\sqrt{K})\sin\beta\sin\delta}{\sin(b\sqrt{K})\sin\alpha\sin\gamma}. \tag{S19}$$

In the Main Text, following the notations in Fig. 2(a), we denote the relationships between adjacent slits in 3×3 SQK tessellations by

$$\cos\beta_i = g_i(\cos\beta_{i+1}). \tag{S20}$$

Meanwhile, the opening angle β_i can also be determined by α_i:

$$\cos\beta_i = \bar{g}[\cos\alpha_i; a_i, b_i, c_i, d_i, K]. \tag{S21}$$

Remind that we have the following complementary relationships:

$$\cos\alpha_i = -\cos\beta_{i+1}. \tag{S22}$$

Combining Eqs. (S20)–(S22), we obtain the expressions of g_i and g_i':

$$g_i(\cos\beta_{i+1}) = \bar{g}[-\cos\beta_{i+1}; a_i, b_i, c_i, d_i, K], \tag{S23}$$

$$g_i'(\cos\beta_{i+1}) = -\bar{g}'[-\cos\beta_{i+1}; a_i, b_i, c_i, d_i, K], \tag{S24}$$

where the index i cycles from 1 to 4.

III. CONVEXITY OF THE LOOP FUNCTION

Analogous to Eqs. (S23) and (S24), we can write the expressions of g_i'':

$$g_i''(\cos\beta_{i+1}) = \bar{g}''[-\cos\beta_{i+1}; a_i, b_i, c_i, d_i, K]. \tag{S25}$$

Taking the derivative of $\bar{g}'$, and combining Eqs. (S3), (S4), (S16), we obtain

$$\bar{g}''[\cos\alpha; a, b, c, d, K] = \bar{k}_g \begin{bmatrix} -\sin(a\sqrt{K})\sin(d\sqrt{K})\sin\alpha\cot\gamma - \sin(b\sqrt{K})\sin(c\sqrt{K})\sin\gamma\cot\alpha \\ -\sin(a\sqrt{K})\sin(b\sqrt{K})\sin\beta\cot\delta - \sin(c\sqrt{K})\sin(d\sqrt{K})\sin\delta\cot\beta \end{bmatrix}, \tag{S26}$$

where the coefficient $\bar{k}_g$ is

$$\bar{k}_g = \frac{\sin\beta\sin\delta\sin(d\sqrt{K})}{\sin^2\alpha\sin^2\gamma\sin^2(b\sqrt{K})\sin(c\sqrt{K})} > 0. \tag{S27}$$

The side lengths a, b, c, d of quadrilateral voids extracted from an SQK strip or tessellation are constrained by $a+b = c+d$, which means that the quadrilateral voids can be determined by two points and two foci of spherical ellipses. Fig. S2 illustrates a spherical ellipse with major axis length $2l$ and focal distance $2f$, satisfying $0 < f\sqrt{K} < l\sqrt{K} < \pi/2$. The foci F_1, F_2 and two points X_1, X_2 on the ellipse determine the spherical quadrilateral $F_2X_1F_1X_2$. We set up a Cartesian coordinate system located at the spherical center $O = (0,0,0)$, such that the coordinates of the foci F_1, F_2 and points X_1, X_2 are given by

$$\begin{aligned} F_1 &= \left(-\sin(f\sqrt{K})/\sqrt{K}, 0, \cos(f\sqrt{K})/\sqrt{K}\right), \\ F_2 &= \left(\sin(f\sqrt{K})/\sqrt{K}, 0, \cos(f\sqrt{K})/\sqrt{K}\right), \\ X_1 &= (x_1, y_1, z_1), \\ X_2 &= (x_2, y_2, z_2). \end{aligned} \tag{S28}$$

The points X_1, X_2 are located at different sides of the plane OF_1F_2, and therefore can be parametrized by $\theta_1 \in (0, \pi)$ and $\theta_2 \in (-\pi, 0)$:

$$\begin{aligned} x_j &= \sin(l\sqrt{K})\cos\theta_j/\sqrt{K}, \\ y_j &= \sqrt{\frac{\sin^2(l\sqrt{K}) - \sin^2(f\sqrt{K})}{\cos^2(f\sqrt{K})}}\sin\theta_j/\sqrt{K}, \\ z_j &= \sqrt{\cos^2\theta_j + \frac{\sin^2\theta_j}{\cos^2(f\sqrt{K})}}\cos(l\sqrt{K})/\sqrt{K}, \end{aligned} \tag{S29}$$

for $j = 1, 2$. Using the locations of vertices F_1, F_2, X_1, X_2, we can obtain the following expressions:

$$\begin{aligned} \sin(d\sqrt{K})\sin(a\sqrt{K})\sin\alpha &= K^{5/2}\left[(F_2 \times X_1) \times (F_2 \times X_2)\right] \cdot F_2, \\ \sin(a\sqrt{K})\sin(b\sqrt{K})\sin\beta &= K^{5/2}\left[(X_1 \times F_1) \times (X_1 \times F_2)\right] \cdot X_1, \\ \sin(b\sqrt{K})\sin(c\sqrt{K})\sin\gamma &= K^{5/2}\left[(F_1 \times X_2) \times (F_1 \times X_1)\right] \cdot F_1, \\ \sin(c\sqrt{K})\sin(d\sqrt{K})\sin\delta &= K^{5/2}\left[(X_2 \times F_2) \times (X_2 \times F_1)\right] \cdot X_2, \end{aligned} \tag{S30}$$

$$\begin{aligned} \sin(d\sqrt{K})\sin(a\sqrt{K})\cos\alpha &= K^2\left(F_2 \times X_1\right) \cdot \left(F_2 \times X_2\right), \\ \sin(a\sqrt{K})\sin(b\sqrt{K})\cos\beta &= K^2\left(X_1 \times F_1\right) \cdot \left(X_1 \times F_2\right), \\ \sin(b\sqrt{K})\sin(c\sqrt{K})\cos\gamma &= K^2\left(F_1 \times X_2\right) \cdot \left(F_1 \times X_1\right), \\ \sin(c\sqrt{K})\sin(d\sqrt{K})\cos\delta &= K^2\left(X_2 \times F_2\right) \cdot \left(X_2 \times F_1\right). \end{aligned} \tag{S31}$$

Substituting Eqs. (S28) and (S30) into the numerator and denominator of the left side of Eq. (S15), we find that

$$\begin{aligned} &\sin(c\sqrt{K})\sin(d\sqrt{K})\sin\delta + \sin(a\sqrt{K})\sin(b\sqrt{K})\sin\beta = (y_1 - y_2)\sqrt{K}\sin(2f\sqrt{K}), \\ &B(\gamma, K)\sin(a\sqrt{K})\sin(d\sqrt{K})\sin\alpha + A(\alpha, K)\sin(b\sqrt{K})\sin(c\sqrt{K})\sin\gamma = (y_1 - y_2)\sqrt{K}\sin(2f\sqrt{K}). \end{aligned} \tag{S32}$$

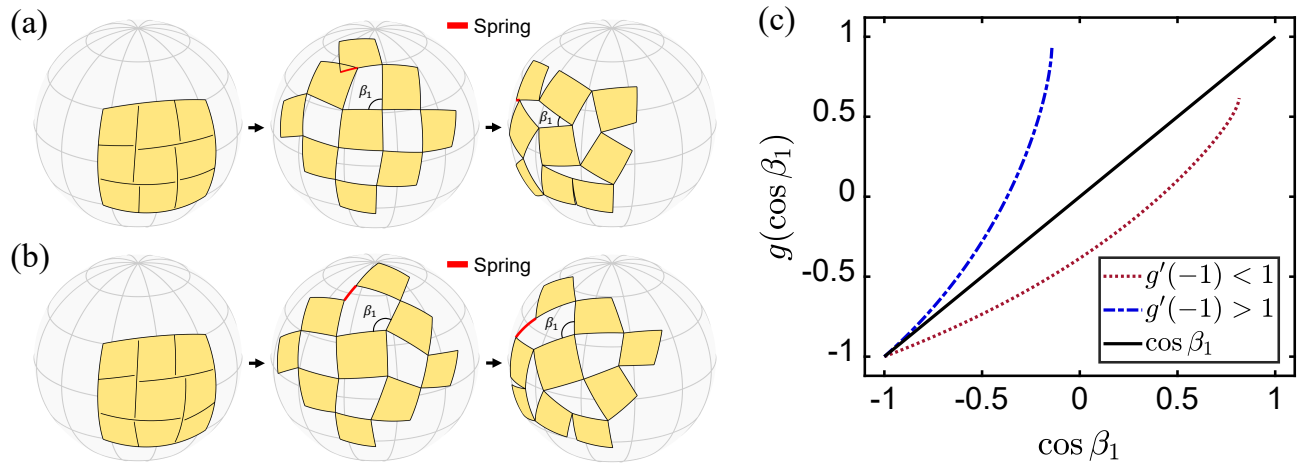

FIG. S3. The 3×3 SQK tessellations with only one compatible state. (a) $g'(-1) < 1$; $\cos\beta_1 = -1$ (left), 0 (middle), 0.816 (right). (b) $g'(-1) > 1$; $\cos\beta_1 = -1$ (left), -0.5 (middle), -0.143 (right). (c) Curves of the loop function $g(\cos\beta_1)$.

Therefore, Eq. (S15) is verified. Now we prove $\bar{g}_i'' > 0$. Substituting Eqs. (S28)–(S31) into Eq. (S26), we can obtain

$$\bar{g}'' = \bar{k}_g \left(\frac{\sin^2(f\sqrt{K}) - \sin^2(l\sqrt{K})}{\sin\theta_1 \sin\theta_2} \right) \frac{t_1^f \cos^2(l\sqrt{K}) + t_2^f \sin^2(l\sqrt{K})}{t_3^f \cos^2(l\sqrt{K}) + t_4^f \sin^2(l\sqrt{K})}. \tag{S33}$$

The coefficient functions are

$$\begin{aligned}
t_1^f =& 4\sin^2(f\sqrt{K})\tan^2(f\sqrt{K})(k_2^f \sin\theta_1 - k_1^f \sin\theta_2)^2 \sin^2\theta_1 \sin^2\theta_2 - \sin^2(f\sqrt{K})(\sin^2\theta_1 - \sin^2\theta_2)^2, \\
t_2^f =& \cos^2(f\sqrt{K}) \left[2\sin^2\theta_1 - \sin^2(\theta_1 - \theta_2) + 2\sin^2\theta_2 \right] \sin^2(\theta_1 - \theta_2), \\
t_3^f =& \sin^2(f\sqrt{K})(k_2^f \sin\theta_1 - k_1^f \sin\theta_2)^2, \\
t_4^f =& -\cos^2(f\sqrt{K}) \sin^2(\theta_1 - \theta_2),
\end{aligned} \tag{S34}$$

where $k_{1,2}^f = \sqrt{\cos^2\theta_{1,2} + \sin^2\theta_{1,2}/\cos^2(f\sqrt{K})}$. Considering $0 < f\sqrt{K} < l\sqrt{K} < \pi/2$, $\theta_1 \in (0, \pi)$, $\theta_2 \in (-\pi, 0)$, we can verify that

$$\frac{\sin^2(f\sqrt{K}) - \sin^2(l\sqrt{K})}{\sin\theta_1 \sin\theta_2} > 0. \tag{S35}$$

$$t_3^f \cos^2(l\sqrt{K}) + t_4^f \sin^2(l\sqrt{K}) = \frac{\sin(a\sqrt{K}) \sin(b\sqrt{K}) \sin(c\sqrt{K}) \sin(d\sqrt{K}) \cos^2(f\sqrt{K}) \sin\alpha \sin\gamma}{\sin^2(l\sqrt{K}) - \sin^2(f\sqrt{K})} > 0, \tag{S36}$$

$$t_2^f = \cos^2(f\sqrt{K}) \begin{bmatrix} 2\sin^2\theta_1 \sin^2\theta_2 + (\sin\theta_1 + \sin\theta_2)^2 \\ + 2(\cos\theta_1 \cos\theta_2 - 1) \sin\theta_1 \sin\theta_2 \end{bmatrix} \sin^2(\theta_1 - \theta_2) > 0, \tag{S37}$$

$$t_1^f \cos^2(f\sqrt{K}) + t_2^f \sin^2(f\sqrt{K}) = 4\sin^2(f\sqrt{K}) \sin^2\theta_1 \sin^2\theta_2 \begin{bmatrix} \cos^2(f\sqrt{K}) \sin^2(\theta_1 - \theta_2) \\ + \sin^2(f\sqrt{K})(k_2^f \sin\theta_1 - k_1^f \sin\theta_2)^2 \end{bmatrix} > 0, \tag{S38}$$

$$t_1^f \cos^2(l\sqrt{K}) + t_2^f \sin^2(l\sqrt{K}) > \min\left\{ t_1^f \cos^2(f\sqrt{K}) + t_2^f \sin^2(f\sqrt{K}), t_2^f \right\} > 0. \tag{S39}$$

As a result, we conclude $\bar{g}'' > 0$. Finally, following Eq. (S25), we prove $g_i'' > 0$. In the Main Text, this result is used to prove the convexity of the loop function g, and to prove that the compatibility condition has at most two roots on the feasible domain $[-1, c_r]$. Examples of 3×3 SQK tessellations with two compatible states are provided in the Main Text. Here we supplement two cases with only one compatible state in Fig. S3.

For the 3×3 SQK tessellations composed of slits with $a_i = c_i$ and $b_i = d_i$, the opening angles satisfy $\alpha_i = \gamma_i$ and $\beta_i = \delta_i$. Thus, we have

$$2\alpha_i + 2\beta_i = 2\pi + 2KS_{\alpha_i}, \tag{S40}$$

and it follows that

$$\cos\beta_i = -\sin(KS_{\alpha_i})\sin\alpha_i - \cos(KS_{\alpha_i})\cos\alpha_i. \tag{S41}$$

In this case, the relationships between opening angles of adjacent slits are denoted by $\cos\beta_i = g_i^e(\cos\beta_{i+1})$. Combining Eqs. (S5)–(S7), and (S41), we can obtain

$$g_i^e(\cos\beta_{i+1}) = \frac{\cos\beta_{i+1}[1+\cos(a_i\sqrt{K})\cos(b_i\sqrt{K})] - \sin(a_i\sqrt{K})\sin(b_i\sqrt{K})}{[1+\cos(a_i\sqrt{K})\cos(b_i\sqrt{K})] - \cos\beta_{i+1}\sin(a_i\sqrt{K})\sin(b_i\sqrt{K})}. \tag{S42}$$

Eq. (S42) can also be written in a compact form:

$$g_i^e(x) = \frac{(P_i+Q_i)x + (P_i-Q_i)}{(P_i+Q_i) + (P_i-Q_i)x}, \tag{S43}$$

where $P_i = \cos^2[(a_i+b_i)\sqrt{K}/2]$ and $Q_i = \cos^2[(a_i-b_i)\sqrt{K}/2]$. Then, the composition of g_i^e and g_j^e can be calculated by

$$g_i^e \circ g_j^e(x) = \frac{(P_iP_j+Q_iQ_j)x + (P_iP_j-Q_iQ_j)}{(P_iP_j+Q_iQ_j) + (P_iP_j-Q_iQ_j)x}. \tag{S44}$$

Finally, we obtain the loop function:

$$g^e(x) = g_1^e \circ g_2^e \circ g_3^e \circ g_4^e(x) = \frac{(P+Q)x + (P-Q)}{(P+Q) + (P-Q)x}, \tag{S45}$$

where $P = \prod_{i=1}^4 P_i$ and $Q = \prod_{i=1}^4 Q_i$.

IV. FORMULATIONS OF THE COMPATIBLE CONFIGURATIONS

We formulate the undeployed $M \times N$ SQK patterns by solving a nonlinear equation system under the given boundary conditions and cut ratios. As illustrated in Fig. S4(a), the slits of an SQK tessellation are divided by their intersecting neighbors into four segments, so that they form quadrilateral voids when deployed. These slits are categorized into horizontal slits [Fig. S4(a), top left] and vertical slits [Fig. S4(a), top right], depending on the opening directions indicated by the blue arrows. The panels are denoted by $P_{i,j}$, and the slits by $C_{i,j}$. For each slit $C_{i,j}$, we systematically denote the side lengths by $a_{i,j}$, $b_{i,j}$, $c_{i,j}$, $d_{i,j}$, and the opening angles by $\alpha_{i,j}$, $\beta_{i,j}$, $\gamma_{i,j}$, $\delta_{i,j}$. The two vertices where the slit $C_{i,j}$ is divided are denoted by $\mathbf{x}_{i,j}$ and $\mathbf{x}'_{i,j}$. In addition, the deployed vertices are denoted by $\mathbf{y}_{i,j}$ and $\mathbf{y}'_{i,j}$. To parameterize the shapes of quadrilateral voids, we use $k^b_{i,j}$ and $k^d_{i,j}$ to denote the ratios by which the slit $C_{i,j}$ is divided by the intersecting slits, i.e., $k^b_{i,j} = b_{i,j}/(a_{i,j}+b_{i,j})$ and $k^d_{i,j} = d_{i,j}/(c_{i,j}+d_{i,j})$. Finally, we define the kinematic parameter $\omega \triangleq \beta_{2,2}$, and use $\omega^\star$ to denote the kinematic parameter at a compatible state.

We establish a Cartesian coordinate system located at the spherical center, so that the positions of vertices can be determined by the spherical coordinates (longitude ϕ and latitude θ) as

$$\begin{aligned}\mathbf{x}_{i,j} &= (\cos\theta_{i,j}\cos\phi_{i,j}, \cos\theta_{i,j}\sin\phi_{i,j}, \sin\theta_{i,j})/\sqrt{K},\\ \mathbf{x}'_{i,j} &= (\cos\theta'_{i,j}\cos\phi'_{i,j}, \cos\theta'_{i,j}\sin\phi'_{i,j}, \sin\theta'_{i,j})/\sqrt{K}.\end{aligned} \tag{S46}$$

We define the function $d_g(\mathbf{v}_1, \mathbf{v}_2) = \arccos[(\mathbf{v}_1\cdot\mathbf{v}_2)/(\|\mathbf{v}_1\|\|\mathbf{v}_2\|)]$ to calculate the scaled geodesic distance between two points $\mathbf{v}_1$ and $\mathbf{v}_2$ on the sphere. Since the slits are geodesic lines, the vertices of an $M \times N$ undeployed SQK pattern should satisfy the following nonlinear constraints

$$\begin{aligned}
\tilde{f}^1_{i,j}(\phi_{k,l},\theta_{k,l},\phi'_{k,l},\theta'_{k,l}) &\triangleq d_g(\mathbf{x}_{i,j},\mathbf{x}'_{i+1,j}) - k^b_{i,j}d_g(\mathbf{x}_{i-1,j},\mathbf{x}'_{i+1,j}) = 0, \quad \mathrm{mod}(i+j,2) = 0,\\
\tilde{f}^2_{i,j}(\phi_{k,l},\theta_{k,l},\phi'_{k,l},\theta'_{k,l}) &\triangleq d_g(\mathbf{x}'_{i,j},\mathbf{x}_{i-1,j}) - k^d_{i,j}d_g(\mathbf{x}'_{i+1,j},\mathbf{x}_{i-1,j}) = 0, \quad \mathrm{mod}(i+j,2) = 0,\\
\tilde{f}^1_{i,j}(\phi_{k,l},\theta_{k,l},\phi'_{k,l},\theta'_{k,l}) &\triangleq d_g(\mathbf{x}_{i,j},\mathbf{x}_{i,j+1}) - k^b_{i,j}d_g(\mathbf{x}'_{i,j-1},\mathbf{x}_{i,j+1}) = 0, \quad \mathrm{mod}(i+j,2) = 1,\\
\tilde{f}^2_{i,j}(\phi_{k,l},\theta_{k,l},\phi'_{k,l},\theta'_{k,l}) &\triangleq d_g(\mathbf{x}'_{i,j},\mathbf{x}'_{i,j-1}) - k^d_{i,j}d_g(\mathbf{x}_{i,j+1},\mathbf{x}'_{i,j-1}) = 0, \quad \mathrm{mod}(i+j,2) = 1,
\end{aligned} \tag{S47}$$

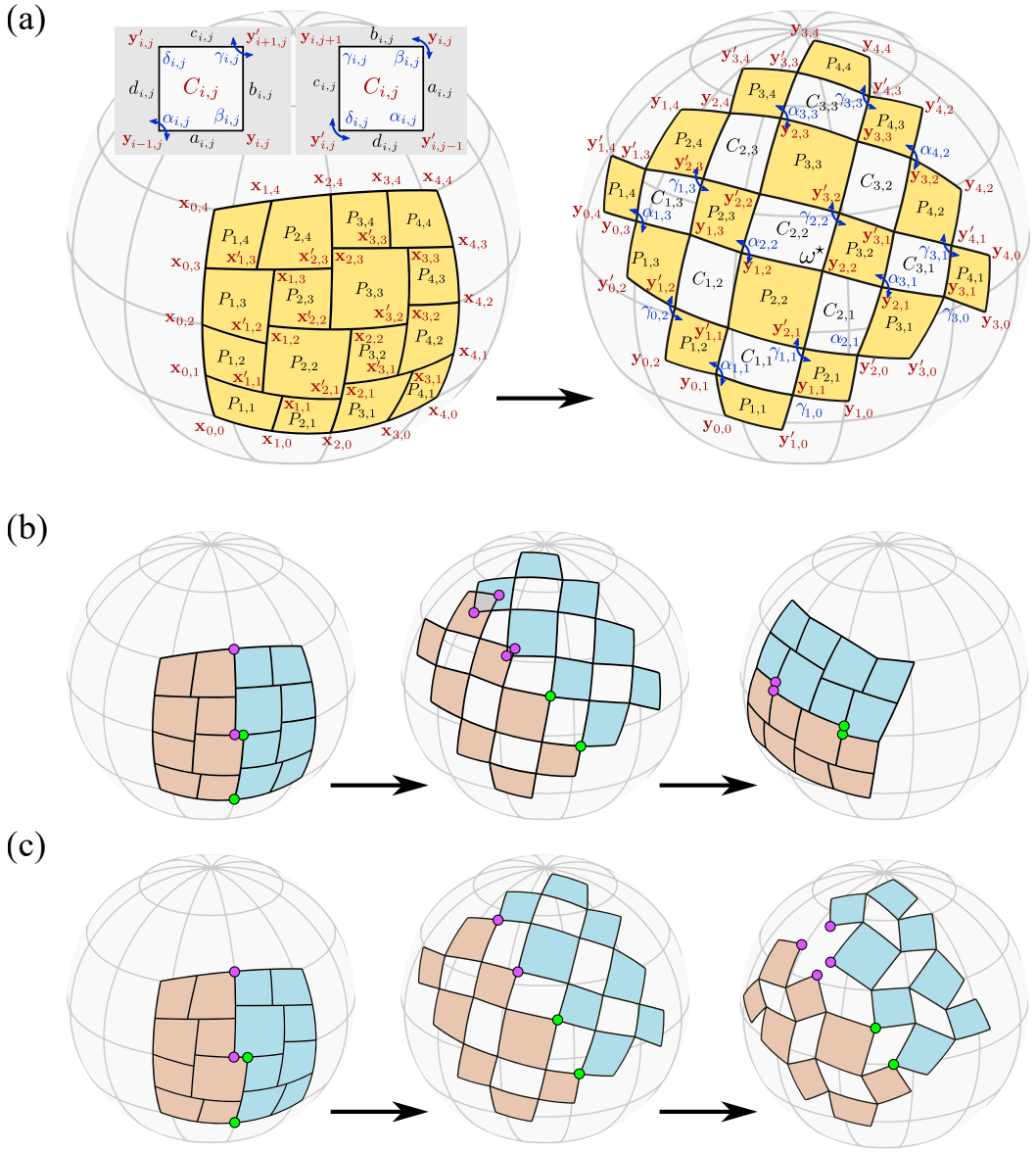

FIG. S4. Kinematics of SQK tessellations. (a) Geometric notations of the undeployed configuration and the deployed configuration of a SQK tessellation. The tessellation is compatible at $\cos\omega^\star = -1, 0$. (b) The SQK tessellation with $k^b_{i,j} = k^d_{i,j}$ has two compatible states at $\cos\omega^\star = \pm 1$. If we disconnect the panels at the purple spots, the tessellation is split into two strips linked at the green spots, and can be rigidly deployed. Each purple spot is divided into two spots (middle), and merge again at $\cos\omega^\star = 1$ (right). (c) The SQK tessellation is optimized to be compatible at $\cos\omega^\star = 0$ (middle). The purple spots split apart when $\cos\omega > 0$ (right).

$$
\begin{aligned}
\hat{f}^1_{i,j}(\phi_{k,l}, \theta_{k,l}, \phi'_{k,l}, \theta'_{k,l}) &\triangleq (\mathbf{x}'_{i+1,j} \times \mathbf{x}_{i,j}) \cdot \mathbf{x}_{i-1,j} = 0, \quad \mathrm{mod}(i+j, 2) = 0, \\
\hat{f}^2_{i,j}(\phi_{k,l}, \theta_{k,l}, \phi'_{k,l}, \theta'_{k,l}) &\triangleq (\mathbf{x}_{i-1,j} \times \mathbf{x}'_{i,j}) \cdot \mathbf{x}'_{i+1,j} = 0, \quad \mathrm{mod}(i+j, 2) = 0, \\
\hat{f}^1_{i,j}(\phi_{k,l}, \theta_{k,l}, \phi'_{k,l}, \theta'_{k,l}) &\triangleq (\mathbf{x}_{i,j+1} \times \mathbf{x}_{i,j}) \cdot \mathbf{x}'_{i,j-1} = 0, \quad \mathrm{mod}(i+j, 2) = 1, \\
\hat{f}^2_{i,j}(\phi_{k,l}, \theta_{k,l}, \phi'_{k,l}, \theta'_{k,l}) &\triangleq (\mathbf{x}'_{i,j-1} \times \mathbf{x}'_{i,j}) \cdot \mathbf{x}_{i,j+1} = 0, \quad \mathrm{mod}(i+j, 2) = 1,
\end{aligned}
\tag{S48}
$$

for $i = 1, ..., M-1$ and $j = 1, ..., N-1$. Eq. (S47) describes the constraints of side-length ratios, and Eq. (S48) restricts that vertices of the same slit are on the same great circle. Fixing the boundary vertices of the tessellation, i.e., $\mathbf{x}^L_j$, $\mathbf{x}^R_j$, $\mathbf{x}^B_i$, and $\mathbf{x}^U_i$ for the left, right, bottom, and upper boundaries, respectively, we can write the boundary

conditions for Eqs. (S47) and (S48) as

$$\begin{aligned}
&\mathbf{x}_{0,j} = \mathbf{x}'_{0,j} = \mathbf{x}_j^L, && \mathrm{mod}(i+j,2) = 0,\\
&\mathbf{x}_{M,j} = \mathbf{x}'_{M,j} = \mathbf{x}_j^R, && \mathrm{mod}(i+j,2) = 0,\\
&\mathbf{x}_{i,0} = \mathbf{x}'_{i,0} = \mathbf{x}_i^B, && \mathrm{mod}(i+j,2) = 1,\\
&\mathbf{x}_{i,N} = \mathbf{x}'_{i,N} = \mathbf{x}_i^U, && \mathrm{mod}(i+j,2) = 1,
\end{aligned} \tag{S49}$$

for $i = 0, 1, ..., M$ and $j = 0, 1, ..., N$. Given the cut ratios $k^b_{i,j}$ and $k^d_{i,j}$, there are two equations and two unknowns (the ϕ and θ coordinates) for each interior vertex $\mathbf{x}_{i,j}$ or $\mathbf{x}'_{i,j}$ according to Eqs. (S47) and (S48), so that the nonlinear equation system is closed. We use the function **fmincon** in Matlab R2020b to solve Eqs. (S47)–(S49). As a result, we can obtain the positions of the interior vertices $\mathbf{x}_{i,j}$ and $\mathbf{x}'_{i,j}$, and consequently the SQK pattern.

In the Main Text, we have proved that the SQK tessellations with $k^b_{i,j} = k^d_{i,j}$ have two compatible states at $\cos\omega^\star = \pm 1$. In what follows, we will shift the latter compatible state from $\cos\omega^\star = 1$ into $\cos\omega^\star \in (-1, 1)$, and construct corresponding SQK tessellations. Firstly, we relax the constraints by disconnecting links between some panels, such that the tailored tessellations become rigidly deployable. For example, Fig. S4(b) illustrates the disconnected links (purple spots) of a 4×4 square SQK tessellation with $k^b_{i,j} = k^d_{i,j} = 0.45$. In general, to relax an $M \times N$ tessellation, we disconnect adjacent panels at the vertices $\mathbf{x}_{2p,2q}$ $(p \geq 1, q \geq 2)$ and $\mathbf{x}'_{2p,2q}$ $(p \geq 1, q \geq 1)$. We use $\mathcal{R}_{i,j}$ to denote the rigid transformations of the panels $P_{i,j}$ relative to the panel $P_{1,1}$. The transformations $\mathcal{R}_{i,j}$ can be calculated by iteratively superimpose the rotation of a panel over its neighbor on the bottom $(j > 1)$, or on the left $(j = 1)$. This procedure can be formulated as follows:

$$\begin{aligned}
&\mathcal{R}_{1,1} = \mathcal{I}, && i = 1,\ j = 1,\\
&\mathcal{R}_{i,1} = \mathbf{R}(\gamma_{i-1,0}, \mathcal{R}_{i-1,1}\mathbf{x}_{i-1,1})\mathcal{R}_{i-1,1}, && \mathrm{mod}(i+1,2) = 1,\ j = 1,\\
&\mathcal{R}_{i,1} = \mathbf{R}(-\alpha_{i-1,1}, \mathcal{R}_{i-1,1}\mathbf{x}'_{i-1,0})\mathcal{R}_{i-1,1}, && \mathrm{mod}(i+1,2) = 0,\ j = 1,\\
&\mathcal{R}_{i,j} = \mathbf{R}(\alpha_{i,j-1}, \mathcal{R}_{i,j-1}\mathbf{x}_{i-1,j-1})\mathcal{R}_{i,j-1}, && \mathrm{mod}(i+j,2) = 1,\ j > 1,\\
&\mathcal{R}_{i,j} = \mathbf{R}(-\gamma_{i-1,j-1}, \mathcal{R}_{i,j-1}\mathbf{x}'_{i,j-1})\mathcal{R}_{i,j-1}, && \mathrm{mod}(i+j,2) = 0,\ j > 1,
\end{aligned} \tag{S50}$$

where $\mathcal{I}$ is the identity transformation, and $\mathbf{R}(\varphi, \mathbf{x}_0)$ is the rotation transformation around $\mathbf{x}_0$ on the sphere, defined by

$$\mathbf{R}(\varphi, \mathbf{x}_0)\mathbf{x} := \frac{\mathbf{x}_0(\mathbf{x}_0 \cdot \mathbf{x})}{\|\mathbf{x}_0\|^2} + \frac{(\mathbf{x}_0 \times \mathbf{x}) \times \mathbf{x}_0}{\|\mathbf{x}_0\|^2}\cos\varphi + \frac{\mathbf{x}_0 \times \mathbf{x}}{\|\mathbf{x}_0\|}\sin\varphi. \tag{S51}$$

For a fixed kinematic parameter $\omega \triangleq \beta_{2,2}$, the opening angles $\alpha_{i,j}, \gamma_{i,j}$ in Eq. (S50) should be solved according to Eqs. (S1), (S2), (S17), (S18), and the following conserved relations:

$$\alpha_{i,j} = \pi - \beta_{i-1,j},\ \gamma_{i,j} = \pi - \delta_{i+1,j},\ \beta_{i,j} = \pi - \gamma_{i,j-1},\ \delta_{i,j} = \pi - \alpha_{i,j+1},\ \mathrm{mod}(i+j,2) = 0. \tag{S52}$$

Then, the displacement field of the tailored SQK tessellation can be written as

$$\mathbf{y} = \mathcal{R}_{i,j}\mathbf{x},\ \mathbf{x} \in P_{i,j}. \tag{S53}$$

Now we can write the conditions for a SQK tessellation to be compatible at $\cos\omega^\star \in (-1, 1)$:

$$\begin{aligned}
&\tilde{h}^1_{p,q}(\phi_{k,l}, \theta_{k,l}, \phi'_{k,l}, \theta'_{k,l}, \omega^\star) \triangleq K\|\mathcal{R}_{2p,2q}\mathbf{x}_{2p,2q} - \mathcal{R}_{2p+1,2q}\mathbf{x}_{2p,2q}\|^2 = 0, && p \geq 1, q \geq 2,\\
&\tilde{h}^2_{p,q}(\phi_{k,l}, \theta_{k,l}, \phi'_{k,l}, \theta'_{k,l}, \omega^\star) \triangleq K\|\mathcal{R}_{2p,2q+1}\mathbf{x}'_{2p,2q} - \mathcal{R}_{2p+1,2q+1}\mathbf{x}'_{2p,2q}\|^2 = 0, && p \geq 1, q \geq 1.
\end{aligned} \tag{S54}$$

Eq. (S54) means that the disconnected panels are linked again at $\cos\omega^\star$, as illustrated in Fig. S4(c). To determine the SQK patterns compatible at $\cos\omega^\star \in (-1, 1)$, we start from an initial pattern with $k^b_{i,j} = k^d_{i,j} = \bar{k}_{i,j}$ (i.e., compatible at $\cos\omega^\star = 1$), then optimize to achieve Eq. (S54). To obtain an optimized pattern close to the input one, we solve the following optimization problem

$$\min_{\phi_{k,l}, \theta_{k,l}, \phi'_{k,l}, \theta'_{k,l}} \begin{cases} (k^b_{i,j} - \bar{k}_{i,j})^2, \\ (k^d_{i,j} - \bar{k}_{i,j})^2, \end{cases} \quad \text{subject to} \begin{cases} \tilde{h}^m_{p,q}(\phi_{k,l}, \theta_{k,l}, \phi'_{k,l}, \theta'_{k,l}, \omega^\star) = 0, \\ \hat{f}^m_{i,j}(\phi_{k,l}, \theta_{k,l}, \phi'_{k,l}, \theta'_{k,l}) = 0, \end{cases} \tag{S55}$$

for $m = 1, 2$. We add the constraints $\hat{f}^m_{i,j} = 0$ [Eq. (S48)] to preserve that vertices of the same slit stay on the same great circle during optimization. The boundary vertices are fixed according to Eq. (S49) in the optimization, so that the corresponding spherical coordinates are not included in the optimization variables. We use the function **fgoalattain** in Matlab R2020b to solve Eq. (S55).

V. PLANAR TESSELLATIONS

If the side lengths of SQK tessellations tend to zero on the unit sphere, the compatibility condition is degenerated to characterize the planar quadrilateral kirigami (PQK) tessellations. Specifically, by applying $K \to 0$, we can obtain the planar forms of Eqs. (S19) and (S33):

$$\tilde{g}'(\cos\alpha; a, b, c, d) = -\frac{d\sin\beta\sin\delta}{b\sin\alpha\sin\gamma}, \tag{S56}$$

$$\tilde{g}'' = \tilde{k}_g \left(\frac{f^2 - l^2}{\sin\theta_1 \sin\theta_2}\right) \frac{\tilde{t}_1^f + \tilde{t}_2^f l^2}{\tilde{t}_3^f + \tilde{t}_4^f l^2}, \tag{S57}$$

where the coefficient $\tilde{k}_g$ is

$$\tilde{k}_g = \frac{d\sin\beta\sin\delta}{b^2 c\sin^2\alpha\sin^2\gamma} > 0. \tag{S58}$$

The coefficient functions are given by

$$\begin{aligned}
\tilde{t}_1^f =& -f^2(\sin^2\theta_1 - \sin^2\theta_2)^2, \\
\tilde{t}_2^f =& \left[2\sin^2\theta_1 - \sin^2(\theta_1 - \theta_2) + 2\sin^2\theta_2\right]\sin^2(\theta_1 - \theta_2), \\
\tilde{t}_3^f =& f^2(\sin\theta_1 - \sin\theta_2)^2, \\
\tilde{t}_4^f =& -\sin^2(\theta_1 - \theta_2).
\end{aligned} \tag{S59}$$

Now suppose that the quadrilateral is not a parallelogram (i.e., $\theta_1 - \theta_2 \neq \pi$). Since $l > f$ and $\tilde{t}_2^f > 0$, we have

$$\tilde{t}_1^f + \tilde{t}_2^f l^2 > \tilde{t}_1^f + \tilde{t}_2^f f^2 = 4f^2\sin^2\theta_1\sin^2(\theta_1 - \theta_2)\sin^2\theta_2 > 0. \tag{S60}$$

$$\tilde{t}_3^f + \tilde{t}_4^f l^2 = \frac{abcd\sin\alpha\sin\gamma}{l^2 - f^2} > 0. \tag{S61}$$

Consequently, we prove $\tilde{g}'' > 0$ for a non-parallelogram quadrilateral void of PQK tessellations. Analogous to the spherical case, this result leads to the strict convexity of the loop function, so that PQK tessellations with non-parallelogram slits also have either one or two compatible configurations.

VI. ENERGETICS

A. Single-spring model

Here we present a single-spring model to simulate the energy landscapes upon the deployment of a 3×3 SQK tessellation. in this model, the panels are rigid and connected by revolute joints, except that one specific joint is replaced by a spring. As shown in Fig. S5(a), we disconnect the vertex above slit C_1, and link the split vertices by a zero-length spring with stiffness k_S. At an incompatible state, the spring will keep shortest elongation to minimize the elastic energy. Thus, the spring and the bottom edge of the flexible panel are always collinear, i.e., on the same great circle. Then, the elongation of the spring is $\Delta_S = |c_1 - \bar{c}_1|$, where $\hat{c}_1$ is the top side length of the slit C_1, and c_1 the bottom edge length of the flexible panel.

In the single-spring model, the elastic energy of a 3×3 SQK tessellation is given by

$$E_S = (k_S/2)(c_1 - \hat{c}_1)^2. \tag{S62}$$

As shown in Fig. S5(b), the diagonal q_1 of the slit C_1 divides β_1 into two angles β_1^L and β_1^R. Following spherical trigonometry, we have

$$\cos(q_1\sqrt{K}) = \cos(a_1\sqrt{K})\cos(d_1\sqrt{K}) + \sin(a_1\sqrt{K})\sin(d_1\sqrt{K})\cos\hat{\alpha}_1, \tag{S63}$$

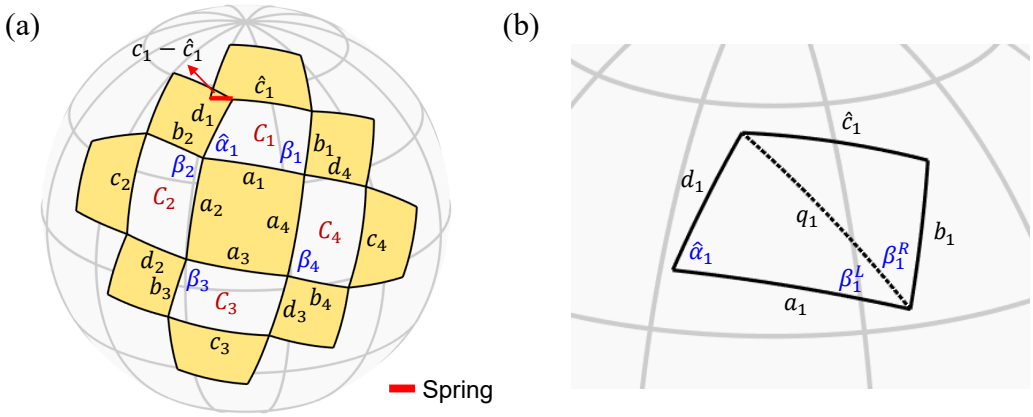

FIG. S5. The single-spring model. (a) The cut-off vertices are linked by a zero-length spring. In this way, at any incompatible state of the 3×3 SQK tessellation, the spring always holds the shortest length to achieve minimum potential energy. (b) The slit C_1 extracted from the tessellation in (a). The diagonal q_1 divides the opening angle β_1 into β_1^L and β_1^R.

$$\sin\beta_1^L = \sin\hat{\alpha}_1 \frac{\sin(d_1\sqrt{K})}{\sin(q_1\sqrt{K})}, \tag{S64}$$

$$\cos\beta_1^L = \frac{\cos(d_1\sqrt{K}) - \cos(a_1\sqrt{K})\cos(q_1\sqrt{K})}{\sin(a_1\sqrt{K})\sin(q_1\sqrt{K})}, \tag{S65}$$

$$\cos(\hat{c}_1\sqrt{K}) = \cos(q_1\sqrt{K})\cos(b_1\sqrt{K}) + \sin(q_1\sqrt{K})\sin(b_1\sqrt{K})\cos\beta_1^R. \tag{S66}$$

Since $\cos\beta_1^R = \cos\beta_1\cos\beta_1^L + \sin\beta_1\sin\beta_1^L$, we substitute Eqs. (S63)–(S65) into Eq. (S66), and obtain

$$\begin{aligned}
\hat{c}_1 = \frac{1}{\sqrt{K}}\arccos\left\{\begin{array}{l}
\sin(b_1\sqrt{K})\sin(d_1\sqrt{K})\left[\sin\hat{\alpha}_1\sin\beta_1 - \cos\hat{\alpha}_1\cos\beta_1\cos(a_1\sqrt{K})\right] \\
+\sin(a_1\sqrt{K})\sin(b_1\sqrt{K})\cos(d_1\sqrt{K})\cos\beta_1 \\
+\cos(b_1\sqrt{K})\left[\cos\hat{\alpha}_1\sin(a_1\sqrt{K})\sin(d_1\sqrt{K}) + \cos(a_1\sqrt{K})\cos(d_1\sqrt{K})\right]
\end{array}\right\}, \\
\hat{\alpha}_1 = \arccos[g_2\circ g_3\circ g_4(\cos\beta_1)],
\end{aligned} \tag{S67}$$

where g_2, g_3, g_4 are given by Eq. (S23). Eq. (S67) gives the explicit expression of $\hat{c}_1$ with respect to $\cos\beta_1$. Therefore, the elastic energy E_S is explicitly determined by the kinematic parameter $\cos\beta_1$.

Now we derive the approximate formulas of the energy E_S when K is small for 3×3 SQK tessellations with equal opposite side lengths of slits, i.e., $c_i = a_i$ and $d_i = b_i$. To be clear, a small K satisfies $L\sqrt{K} \ll 1$ for $L = \max\{a_1, b_1, ..., a_4, b_4\}$. In this case, we calculate the Taylor series of $\hat{c}_1/b_1$ following Eq. (S67):

$$\frac{\hat{c}_1}{b_1} = \frac{c_1}{b_1} - \frac{1}{2}\sum_{i=1}^{4}(a_i b_i)K\sin^2\beta_1 + O[L^4K^2]. \tag{S68}$$

Thus, the scaled energy $E_S/(k_S b_1^2)$ can be approximated by

$$\frac{E_S}{k_S b_1^2} = \frac{1}{8}\left[\sum_{i=1}^{4}(a_i b_i)\right]^2 K^2\sin^4\beta_1 + O[L^6K^3]. \tag{S69}$$

Additionally, we can calculate the Taylor series of the loop function $g^e(\cos\beta_1)$ based on Eq. (S45):

$$g^e(\cos\beta_1) = \cos\beta_1 - \frac{1}{2}\sum_{i=1}^{4}(a_i b_i)K\sin^2\beta_1 + O[L^4K^2]. \tag{S70}$$

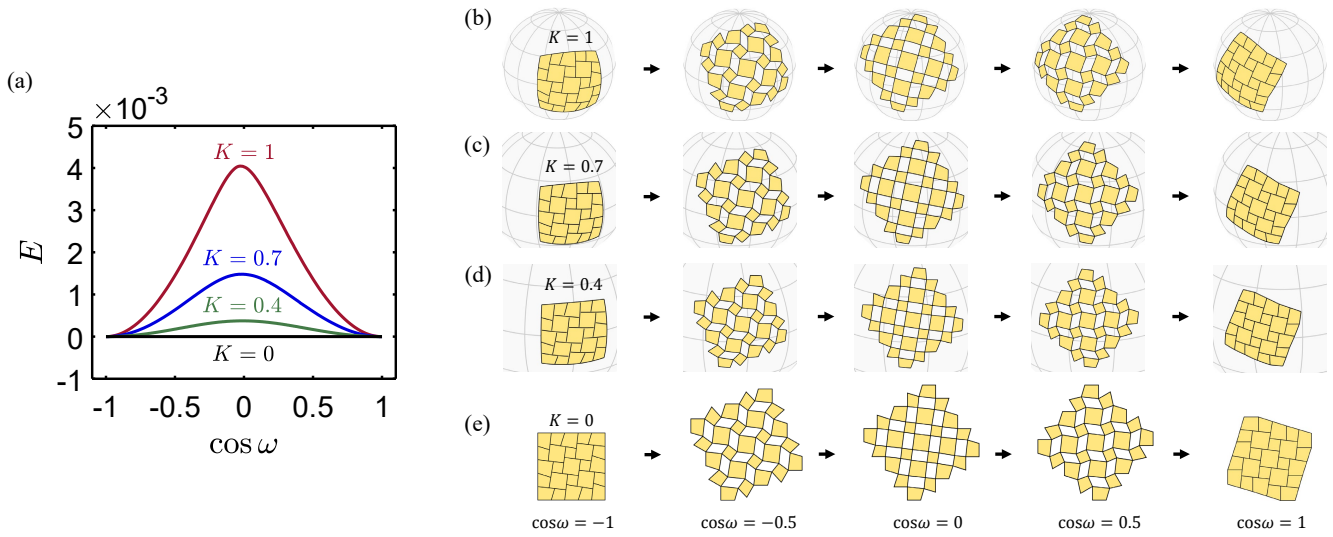

FIG. S6. (a) The evolution of elastic energy E of 5×5 SQK and PQK shells with equal opposite side lengths of slits in respect of the kinematic parameter $\cos\omega$. The square shells have the same side length $s = \pi/3$ but decreasing Gaussian curvatures $K = 1$, 0.7, 0.4, and 0. The aspect ratios of the slits are fixed as 0.4. (b)–(d) The deployment path of the SQK shells. The configurations for different $\cos\omega$ are determined by minimizing the elastic energy of the multispring model. (e) The deployment path of the PQK shell.

Comparing Eqs. (S68) and (S70), we obtain

$$\frac{\Delta_S}{b_1} = \frac{|\hat{c}_1 - c_1|}{b_1} = |g^e(\cos\beta_1) - \cos\beta_1| + O[L^4K^2]. \tag{S71}$$

Finally, we obtain the scaled energy expressed by the loop function:

$$\frac{E_S}{k_S b_1^2} = \frac{1}{2}[g^e(\cos\beta_1) - \cos\beta_1]^2 + O[L^6K^3]. \tag{S72}$$

B. Multispring model

For a general $M \times N$ SQK tessellation, we assume the hinge-connected panels are made of elastic materials. To simulate the deformation of the panels, we use a multispring model, in which the vertices are linked by springs along the edges and diagonals of panels. Then, the elastic energy of the deployed tessellations can be written as

$$\begin{aligned} E(\mathbf{Y}) &= \sum_n \frac{k_n}{2}\left[l_n(\mathbf{Y}) - l_n^0\right]^2, \\ \mathbf{Y} &= \left\{\mathbf{y}_{i,j}, \mathbf{y}'_{i,j} | i = 0,1,...,M, j = 0,1,...,N\right\}, \end{aligned} \tag{S73}$$

where $\mathbf{Y}$ is the array consisting of all the vertex positions of panels, l_n the spring length indexed by n, l_n^0 the rest spring length for the undeployed tessellation, and k_n the spring stiffness. For simplicity, we set $k_n = 1/l_n^0$ in our demonstration. We define the function

$$\eta(\mathbf{v}_1, \mathbf{v}_2, \mathbf{v}_3) = \frac{\mathbf{v}_1 \times \mathbf{v}_2}{\|\mathbf{v}_1 \times \mathbf{v}_2\|} \cdot \frac{\mathbf{v}_3 \times \mathbf{v}_2}{\|\mathbf{v}_3 \times \mathbf{v}_2\|} \tag{S74}$$

so that the kinematic parameter $\cos\omega$ can be expressed as $\cos\omega \triangleq \cos\beta_{2,2} = \eta(\mathbf{y}_{1,2}, \mathbf{y}_{2,2}, \mathbf{y}'_{3,2})$. We use the spherical coordinates (longitude $\tilde{\phi}$ and latitude $\tilde{\theta}$) to represent the vertices

$$\mathbf{y}_{i,j} = (\cos\tilde{\theta}_{i,j}\cos\tilde{\phi}_{i,j}, \cos\tilde{\theta}_{i,j}\sin\tilde{\phi}_{i,j}, \sin\tilde{\theta}_{i,j})/\sqrt{K}, \tag{S75}$$

$$\mathbf{y}'_{i,j} = (\cos\tilde{\theta}'_{i,j}\cos\tilde{\phi}'_{i,j}, \cos\tilde{\theta}'_{i,j}\sin\tilde{\phi}'_{i,j}, \sin\tilde{\theta}'_{i,j})/\sqrt{K}. \tag{S76}$$

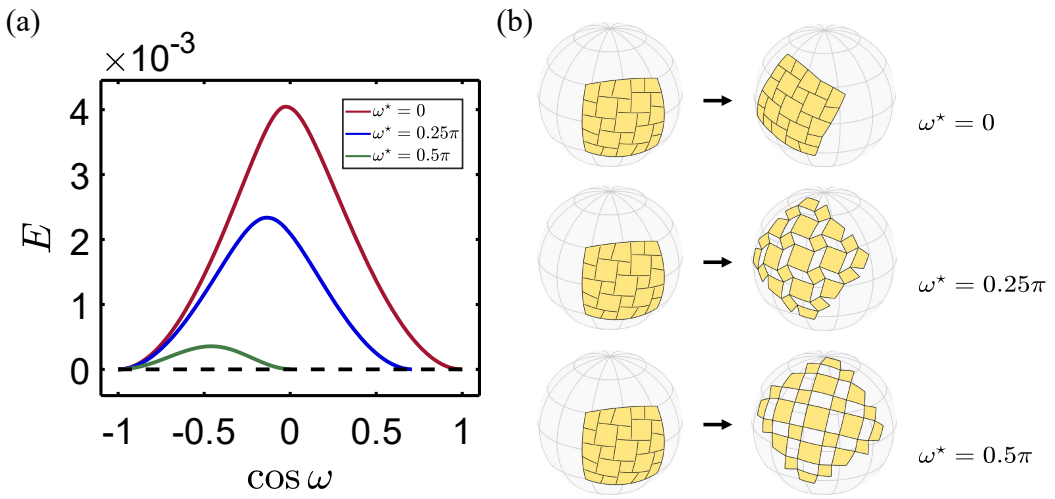

FIG. S7. (a) The evolution of elastic energy E of 5×5 SQK tessellations as a function of the kinematic parameter $\cos\omega$. (b) The SQK tessellations have the same side length $s = \pi/3$ and Gaussian curvature $K = 1$. They are designed to be compatible at $\cos\omega = \cos\omega^\star = 0,\ 1/\sqrt{2}$, and 1, respectively.

To determine the vertex coordinates of deformed SQK tessellations, we start from the undeployed state at $\cos\omega = -1$, increase $\cos\omega$ incrementally, and minimize the elastic energy Eq. (S73) at each step by optimizing the positions of the vertices $\mathbf{y}_{i,j}$ and $\mathbf{y}'_{i,j}$ on the sphere. We use the function **fmincon** in Matlab R2020b to solve the following optimization problem

$$\min_{\tilde{\phi}_{k,l},\tilde{\theta}_{k,l},\tilde{\phi}'_{k,l},\tilde{\theta}'_{k,l}} E\left(\mathbf{y}_{i,j},\mathbf{y}'_{i,j}\right) \text{ subject to } \begin{cases} [\eta(\mathbf{y}_{1,2},\mathbf{y}_{2,2},\mathbf{y}'_{3,2}) - \cos\omega]^2 = 0, \\ \left(\tilde{\phi}_{1,1} - \bar{\phi}_{1,1}\right)^2 = 0, \left(\tilde{\theta}_{1,1} - \bar{\theta}_{1,1}\right)^2 = 0, \left(\tilde{\phi}_{1,2} - \bar{\phi}_{1,2}\right)^2 = 0. \end{cases} \tag{S77}$$

In this optimization, we use $(\bar{\phi}_{0,0}, \bar{\theta}_{0,0}, \bar{\phi}_{0,1})$ to express the orientation of the tessellation on the sphere.

In Fig. S6, we illustrate the energy evolution upon deployment of square SQK and PQK tessellations of the same side length but different Gaussian curvatures $K = 1,\ 0.7,\ 0.4$, and 0. The configurations of these tessellations on the deployment path are also provided. In Fig. S7, we illustrate the energy evolution upon deployment of square SQK tessellations designed to be compatible at $\cos\omega = \cos\omega^\star = 0,\ 1/\sqrt{2}$, and 1, respectively. One can observe that each energy curve has two zero points. Moreover, the energy barrier is lower if the two compatible states of a tessellation are closer to each other.

VII. INVERSE DESIGN

In this section, we aim to optimize a square SQK tessellation on a unit sphere to achieve a domelike shape at a certain deployed state. The design problem can be formulated by minimizing the distance between the target curve and outer vertices at the deployed state over the domain of vertex locations on the sphere. For example, consider an $N \times N$ square SQK pattern ($N = 6$, $k_{i,j} \approx k'_{i,j} \approx 0.5$) with side length s. the corners of the square can be given by

$$\begin{aligned} \mathbf{x}^{LB} &= (\cos\theta_0\cos\phi_0,\ -\cos\theta_0\sin\phi_0,\ -\sin\theta_0), \\ \mathbf{x}^{RB} &= (\cos\theta_0\cos\phi_0,\ \cos\theta_0\sin\phi_0,\ -\sin\theta_0), \\ \mathbf{x}^{RU} &= (\cos\theta_0\cos\phi_0,\ \cos\theta_0\sin\phi_0,\ \sin\theta_0), \\ \mathbf{x}^{LU} &= (\cos\theta_0\cos\phi_0,\ -\cos\theta_0\sin\phi_0,\ \sin\theta_0), \end{aligned} \tag{S78}$$

where $\theta_0 = s/2$ and $\phi_0 = \arcsin(\tan(s/2))$. The boundary vertices are determined by four series of parameters:

$$\begin{aligned} \mathbf{x}_i^B &= \mathbf{R}(t_i^B s, \mathbf{x}^{LB} \times \mathbf{x}^{RB})\mathbf{x}^{LB}, \\ \mathbf{x}_i^U &= \mathbf{R}(t_i^U s, \mathbf{x}^{LU} \times \mathbf{x}^{RU})\mathbf{x}^{LU}, \\ \mathbf{x}_i^L &= \mathbf{R}(t_i^L s, \mathbf{x}^{LB} \times \mathbf{x}^{LU})\mathbf{x}^{LB}, \\ \mathbf{x}_i^R &= \mathbf{R}(t_i^R s, \mathbf{x}^{RB} \times \mathbf{x}^{RU})\mathbf{x}^{RB}, \end{aligned} \tag{S79}$$

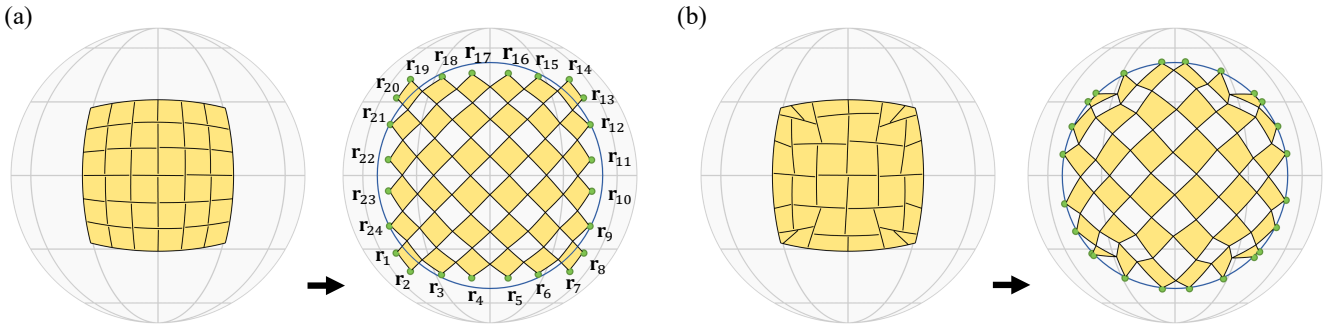

FIG. S8. Shape morphing of a square SQK tessellation. (a) The square SQK tessellation with side length $s = 0.3\pi$ and Gaussian curvature $K = 1$ is deployed ($\omega^\star = 0.5\pi$) to align with a small circle at $x = 0.65$. (b) The optimized SQK tessellation approximates the circle.

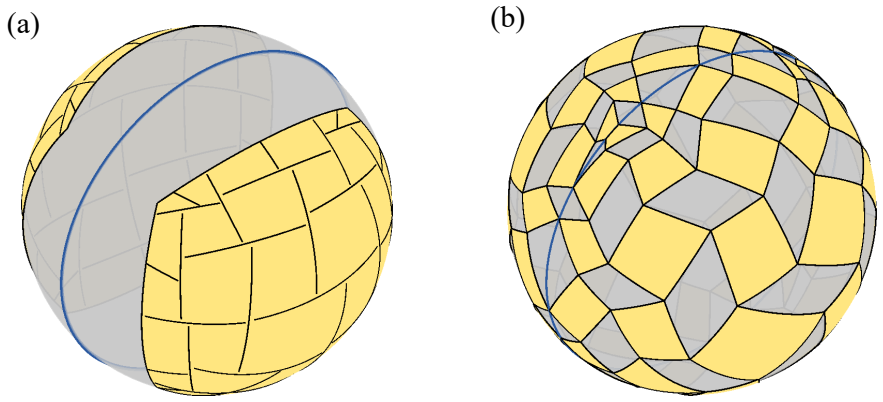

FIG. S9. Two mirror-symmetrical reconfigurable SQK shell structures optimized to approximate hemispheres can be connected to form a full sphere. (a) Each kirigami pattern is perforated on a spherical square of side length $s = 0.45\pi$ and Gaussian curvature $K = 1$. (b) Each deployed configuration covers a hemispherical dome of height $h = 1.0$, and is connected to compose a full sphere.

where $i = 0, 1, ..., N$, $0 = t_0^I < t_1^I < ... < t_N^I = 1$, $I = L, R, B, U$. The outer vertices at the deployed compatible state are denoted by $\mathbf{r}_n = (x_n, y_n, z_n)$, for $n = 1, 2, ..., 4N$, highlighted by green dots in Fig. S8(a). The equation of a circle on the unit sphere can be given by $\tilde{g}(\mathbf{r}, \lambda) = x - \lambda$ for $\mathbf{r} = (x, y, z)$. We use the parameter $\lambda \in (-1, 1)$ to control the size and location of the target circle. To characterize the distance between the target circle and the outer vertices $\mathbf{r}_n$ for a fixed kinematic parameter $\omega = \omega^\star$, we define the following function:

$$\tilde{g}_{i,j}(\phi_{k,l}, \theta_{k,l}, \phi'_{k,l}, \theta'_{k,l}, \lambda, \mathbf{R}, \omega^\star) = [\tilde{g}(\mathbf{R}\mathbf{r}_m, \lambda)]^2, \tag{S80}$$

where $\phi_{k,l}, \theta_{k,l}, \phi'_{k,l}, \theta'_{k,l}$ are spherical coordinates of the vertices $\mathbf{x}_{i,j}$ and $\mathbf{x}'_{i,j}$ on the undeployed tessellation, and $\mathbf{R} = \mathbf{R}(\varphi, \mathbf{x}_0)$ the rotation transformation controlling the orientation of the tessellation. We approximate a circle with $\lambda = \lambda_0$ by tackling the following optimization problem:

$$\min_{\phi_{k,l},\, \theta_{k,l},\, \phi'_{k,l},\, \theta'_{k,l},\; t_k^I,\; \lambda,\; \mathbf{R}} (\lambda - \lambda_0)^2 \text{ subject to } \begin{cases} \tilde{g}_{i,j}(\phi_{k,l}, \theta_{k,l}, \phi'_{k,l}, \theta'_{k,l}, \lambda, \mathbf{R}, \omega^\star) = 0, \\ \tilde{h}^m_{p,q}(\phi_{k,l}, \theta_{k,l}, \phi'_{k,l}, \theta'_{k,l}, \omega^\star) = 0, \\ 0 = t_0^I < t_1^I < ... < t_N^I = 1. \end{cases} \tag{S81}$$

The constraints $\hat{f}^m_{i,j} = 0$ restrict that the vertices of the same slits locating on the same great circle [Eq. (S48)]. The constraints $\tilde{h}^m_{p,q} = 0$ preserve the compatibility [Eq. (S54)]. We use the function **fgoalattain** in Matlab R2020b to solve Eq. (S81). The optimized tessellation approximating a small circle is illustrated in Fig. S8(b).

For the demonstration in Fig. 4 in the Main Text, the input of the optimization is a 6×6 square SQK tessellation of side length $s = 0.465\pi$ and Gaussian curvature $K = 1$. The initial tessellation is set to be compatible at $\omega^\star = 0.6\pi$, which is obtained from Eqs. (S47)–(S49) and (S55) with constant cut ratios $k^b_{i,j} = k^d_{i,j} = 0.5$ and uniformly distributed

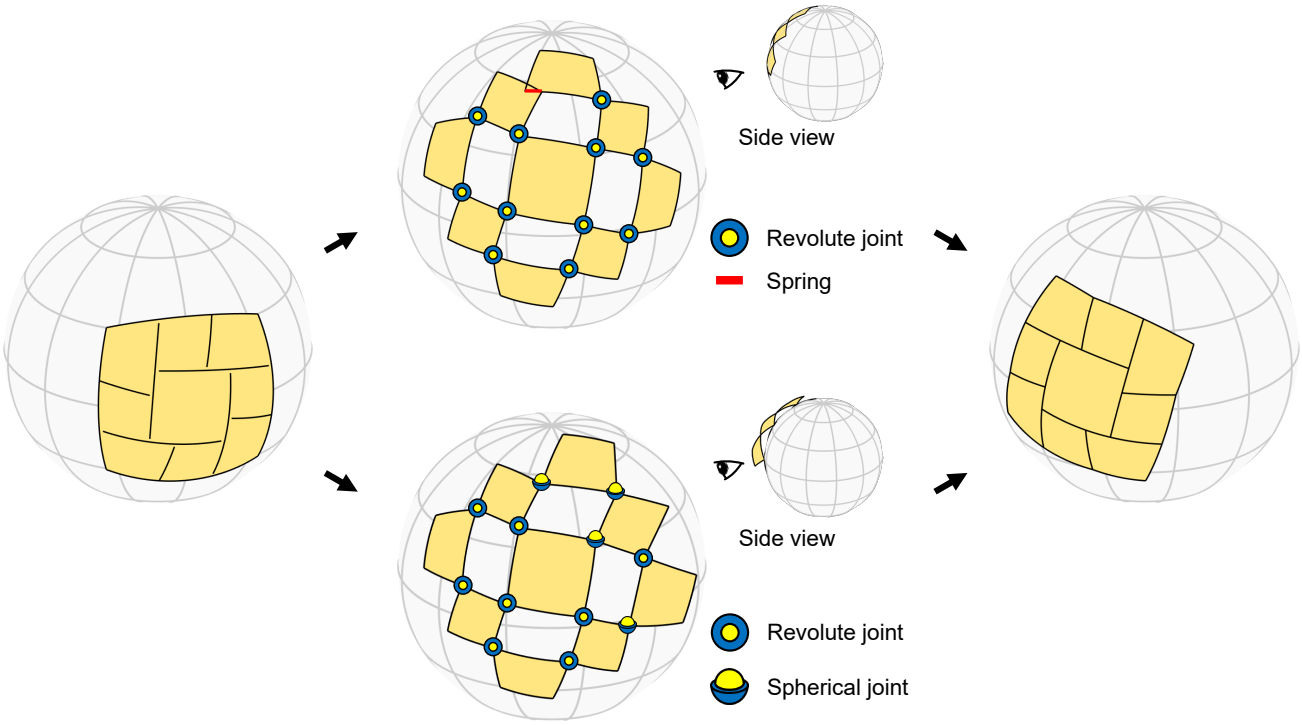

FIG. S10. The apparent rigidity of the two-configuration result will vanish if we introduce additional freedom to move in the radial direction. Middle top: the single-spring model incorporates revolute joints and a spring to achieve the transition between two compatible configurations. Middle bottom: spherical joints can be used to permit some panels to move out of the spherical surface, such that zero-energy transition can be realized.

boundary vertices. The height of the target spherical dome is $h = 1.2$, such that the equation of the boundary circle is $\tilde{g}(\mathbf{r}, \lambda_0) = x - \lambda_0$ with $\lambda_0 = -0.2$. As an additional demonstration, we optimize to obtain a square SQK shell with side length $s = 0.45\pi$ that approximates a hemispherical dome ($\lambda_0 = 0$) at $\omega^\star = 0.7\pi$. Then we can connect the designed structure and its counterpart with mirror symmetry to achieve a full deployed sphere, as shown in Fig. S9.

VIII. THE ROLE OF OUT-OF-SURFACE MOTION

In the main text, we use the single-spring model and the multispring model to simulate the transition between two compatible configurations of the SQK tessellations. Essentially, both of these two models introduce elastic energy at the incompatible states to make the transition happen, during which the panels can only move on the spherical surface. As an realization, the panels can be connected by revolute joints that only permit the rotation around the radial direction of the spherical surface. Here we supplement a mechanism model that replaces some of the revolute joints by spherical joints to realize zero-energy transition between two compatible configurations. The difference is that the spherical joints allow the panels to have deformations out of the spherical surface. As shown in Fig. S10, the three panels on the right of the kirigami tessellation can move out of the spherical surface by adding four spherical joints, and the tessellation becomes a floppy mechanism with additional degrees of freedom of motion. In this case, the incompatibility of SQK tessellations are characterized by the out-of-surface motion instead of rigidity. For SQK tessellations composed of more panels, it is possible to replace carefully-chosen revolute joints by spherical joints to systematically design such mechanisms of SQK tessellations with out-of-surface motion. We leave this as future work.

IX. FABRICATION OF PHYSICAL MODELS

The 5×5 SQK tessellation [shown in Figs. 1(c) and 1(d) in the Main Text] is fabricated by the 3D printer Stratasys Objet350 Connex3 with the material TangoBlack. The panels are connected by the rubber-like materials at the joints.

The 6×6 SQK dome [shown in Figs. 4(c) and 4(d) in the Main Text] is fabricated by the 3D printer ZRapid

iSLA1900D with the material 9400 Resin. The panels are connected by revolute joints.

X. MOVIE CAPTION

Movie 1 *Configuration transition of the bistable spherical kirigami domelike structure.*